Key Points:
- Topographic depressions did not consistently act as nitrous oxide hot spots, with controls on fluxes varying over the growing season
- Cold spring temperatures limit soil respiration that depletes dissolved oxygen to induce nitrous oxide production by denitrification
- Large summer rainfall events may not stimulate soil nitrous oxide emissions, even from topographic depressions, when soil moisture is low

Correspondence to:
A. H. Krichels,
krichel2@illinois.edu

Dynamic Controls on Field-Scale Soil Nitrous Oxide Hot Spots and Hot Moments Across a Microtopographic Gradient

Alexander H. Krichels[1] (iD) **and Wendy H. Yang[1,2,3]** (iD)

[1]Program in Ecology, Evolution, and Conservation Biology, University of Illinois, Urbana, IL, USA, [2]Department of Plant Biology, University of Illinois, Urbana, IL, USA, [3]Department of Geology, University of Illinois, Urbana, IL, USA

Abstract Soil nitrous oxide (N_2O) emissions are highly variable in space and time, making it difficult to estimate ecosystem level fluxes of this potent greenhouse gas. While topographic depressions are often evoked as permanent N_2O hot spots and rain events are well-known triggers of N_2O hot moments, soil N_2O emissions are still poorly predicted. Thus, the objective of this study was to determine how to best use topography and rain events as variables to predict soil N_2O emissions at the field scale. We measured soil N_2O emissions 11 times over the course of one growing season from 65 locations within an agricultural field exhibiting microtopography. We found that the topographic indices best predicting soil N_2O emissions varied by date, with soil properties as consistently poor predictors. Large rain events (>30 mm) led to an N_2O hot moment only in the early summer and not in the cool spring or later in the summer when crops were at peak growth and likely had high evapotranspiration rates. In a laboratory experiment, we demonstrated that low heterotrophic respiration rates at cold temperatures slowly depleted soil dissolved O_2, thus suppressing denitrification over the 2–3 day timescale typical of field ponding. Our findings show that topographic depressions do not consistently act as N_2O hot spots and that rainfall does not consistently trigger N_2O hot moments. We assert that the spatiotemporal variation in soil N_2O emissions is not always characterized by predictable hot spots or hot moments and that controls on this variation change depending on environmental conditions.

Plain Language Summary Soils are the primary source of nitrous oxide (N_2O), a greenhouse gas that contributes to global warming. Nitrous oxide is produced under oxygen-depleted conditions that can occur when soils are saturated with water. Large rain events are therefore thought to lead to short periods of high soil N_2O emissions. Landscape topography can shape spatial patterns in soil moisture and other soil properties that may regulate spatial variation in soil N_2O emissions. The goals of this study were to determine which topographic factors best predict spatial variation in soil N_2O emissions and under what conditions, and to determine when large rain events may not lead to bursts of soil N_2O emissions. We found that throughout the growing season, all topographic indices were poor predictors of soil N_2O emissions in an agricultural field. A large early summer rain event triggered a pulse of soil N_2O emissions, but large rain events did not trigger similar pulses in the cool spring months or later in the summer when the crops were at peak growth with high soil water demand. This has important implications for predicting how soil N_2O emissions will respond to expected future changes in temperature and rainfall, feeding back on climate change.

1. Introduction

Soil nitrous oxide (N_2O) emissions are highly variable in space and time, making it difficult to estimate ecosystem level fluxes of this potent greenhouse gas. High rates of N_2O emissions occur from discrete areas in space (hot spots) and short periods of time (hot moments) that disproportionately contribute to cumulative landscape scale N_2O emissions (Bernhardt et al., 2017; Groffman et al., 2009; McClain et al., 2003). The majority of N_2O emitted from soils is derived from denitrification (Ciais et al., 2013), an anaerobic process in which nitrate (NO_3^-) is sequentially reduced to N_2O and then to inert nitrogen gas (N_2; Knowles, 1982). Under increasingly anaerobic conditions coupled to high C availability, the proportion N_2 to N_2O produced from denitrification increases, potentially limiting net N_2O emissions to the atmosphere (Chapuis-Lardy et al., 2007; Knowles, 1982). Rain events can saturate soils with water, facilitating a

decrease in soil O_2 concentrations if standing water inhibits diffusive resupply of O_2 consumed by microbial respiration (Estop-Aragonés et al., 2013; Takai & Kamura, 1966), thus triggering hot moments in N_2O production via denitrification (Dobbie et al., 2003; Li et al., 1992; Molodovskaya et al., 2012; Sexstone et al., 1985). Similarly, water accumulation in topographic depressions can drive down soil O_2 concentrations (Krichels et al., 2019 Le et al., 2015; Sophocleous, 2002), forming hot spots of N_2O emissions (Turner et al., 2016; Velthof et al., 2009; Yanai et al., 2003). While topographic depressions and rain events are often invoked conceptually as drivers of hot spots and hot moments of denitrification, it is unclear how to best use these variables to predict N_2O emissions.

Topographic depressions can be characterized using a variety of approaches that relate differently to how N_2O hot spots are formed. Light detection and ranging (LIDAR) data can be used to create fine-scale digital terrain models (DTMs) that predict patterns in soil moisture as a result of gravity-driven lateral transport of water (Fink & Drohan, 2016; Li et al., 2018; Turner et al., 2016). However, absolute elevation may not predict N_2O hot spots in local depressions, which might accumulate water after relatively small rain events. Topographic fill models derived from DTMs can identify these discrete, localized areas lower in elevation relative to the surrounding terrain. Alternatively, soil properties can record a history of hydrological flow paths driven by topography (Burke et al., 1989; Schimel et al., 1985; Suriyavirun et al., 2019) and also incorporate factors beyond the role of hydrological flow in forming N_2O hot spots. For example, clay transport downslope into depositional areas can lead to the development of clay-rich soils with high water retention conducive to sustaining hypoxic denitrification hot spots (Fissore et al., 2017). Soil magnetic susceptibility, which results from magnetic mineral dissolution in response to prolonged exposure to anaerobic conditions (Grimley et al., 2004), could also act as a direct record of historical soil redox regimes that could shape microbial communities with different functional potentials (DeAngelis et al., 2010; Pett-Ridge et al., 2006; Suriyavirun et al., 2019). While there are many approaches to predicting the locations of N_2O hot spots, past studies have focused on using indices derived from DTMs, which have yielded only modest predictive power (Li et al., 2012; Turner et al., 2016).

Topography-mediated soil drainage can also indirectly alter soil N_2O emissions by changing soil properties that directly control denitrification dynamics. Carbon (C) can accumulate in depressional areas through erosion (Nitzsche et al., 2017) or as a result of slowed decomposition under hypoxic conditions (Linn & Doran, 1984). Carbon compounds are oxidized during the heterotrophic process of denitrification, so higher C concentrations may lead to enhanced denitrification rates in depressional areas. Indeed, soil C concentrations are often correlated to N_2O emissions at the field scale (Li et al., 2012; Milne et al., 2011; Velthof et al., 1996; Yanai et al., 2003). Repeated saturation of soils can also lead to increases in pH (De-Campos et al., 2009), creating a variation in pH across topographic gradients (Suriyavirun et al. 2019). Soil pH also exerts a strong effect on denitrification dynamics, with higher N_2O emissions observed in slightly acidic soils (Knowles, 1982; Milne et al., 2011; Russenes et al., 2016; Yanai et al., 2003). However, the effects of pH on N_2O dynamics are complicated as elevated pH leads to increased denitrification rates and also increases the proportion of N_2O that is reduced to inert N_2 (Knowles, 1982). While other factors can lead to spatial variation in soil organic C and pH, topography may be the most important factor driving this variability in homogenously managed agricultural fields. Uneven distribution of soil C and pH across topographic gradients may accentuate hot spots of denitrification following rain events and could drive spatial patterns in N_2O emissions in-between rain events when topography does not lead to patterns in soil moisture.

Although topographic depressions are often characterized as N_2O hot spots (Ambus & Christensen, 1994; Saha et al., 2017; Turner et al., 2016; Yanai et al., 2003), they may not always act as hot spots in response to large precipitation events. In some cases, depressional areas may only act as hot spots in between rather than after rain events, with upslope areas acting as postrain hot spots (Krichels et al., 2019). This has been observed throughout the growing season under a range of soil inorganic N concentrations (Krichels et al., 2019). Rather than depleted soil O_2 and increased soil C availability driving hot spots of denitrification in topographic depressions (Li et al., 2012; Milne et al., 2011; Turner et al., 2016; Velthof et al., 1996; Yanai et al., 2003), differences in soil biotic and abiotic properties may cause depressional and upslope areas to have distinct controls over denitrification rates (Krichels et al., 2019; Suriyavirun et al., 2019). For example, microbial community composition can differ between soils that experience different fluctuations in soil O_2 concentrations (DeAngelis et al., 2010). Given that the composition of denitrifying

microbial communities can affect denitrification rates (Graham et al., 2014, 2016; Philippot & Hallin, 2005), differing denitrifier communities in depressional versus upslope areas may have distinct responses to precipitation events (Suriyavirun et al. 2019; Krichels et al. 2019). Furthermore, upslope soils can have a greater proportion of macroaggregates compared with depressional soils (De-Campos et al., 2009; Horn & Smucker, 2005; Six et al., 2004), potentially connecting aerobic and anaerobic soil microsites following large rain events (Algayer et al., 2014; Askaer et al., 2010; Sey et al., 2008) and allowing aerobic nitrification to continuously supply NO_3^- to fuel nearby denitrifiers (Krichels et al., 2019; Palta et al., 2016) via coupled nitrification-denitrification (Baldwin and Mitchell, 2000; Kool et al., 2010). Together, these factors can act as soil drainage legacy effects that cause the location of N_2O hot spots within a field to be dynamic in response to recent precipitation.

Rain events are often thought of as triggers for hot moments of N_2O emissions to occur across landscapes and in depressional areas (Dobbie & Smith, 2003; Molodovskaya et al., 2012; Sexstone et al., 1985), especially in agricultural fields where inorganic N concentrations remain high throughout the growing season (Sebilo et al., 2013). However, seasonal changes in temperature and crop growth could constrain this response. For example, depressional areas may not act as hot spots of denitrification in the cold springtime because cold conditions can prevent the depletion of O_2 dissolved in soil pore water. In order to create hypoxic conditions that stimulate denitrification, microbial respiration must consume O_2 dissolved in soil pore water (Estop-Aragonés et al., 2013; Takai & Kamura, 1966). While large rain events can flush O_2 out of soil pores in temperate upland soils (Jarecke et al., 2016), particularly in depressional areas (Krichels et al. 2019), dissolved O_2 may persist in inundated soils under cold conditions in the spring when soils are still cold because rates of microbial respiration are highly sensitive to soil temperature (Davidson et al., 2012). In general, microbial processes are also likely to be inhibited under cold temperatures, including denitrification (Goodroad & Keeney, 1984; Holtan-Hartwig et al., 2002; Maag & Vinther, 1996), which may further limit N_2O production in response to spring precipitation. Furthermore, microbial community composition can change seasonally in response to changes in temperature (Andrews et al., 2000; Bradford et al., 2008; Zogg et al., 1997) and crop growth (Buyer et al., 2002; Mbuthia et al., 2015), and denitrifying microorganisms may be more active at different points of the growing season. As such, the activation of hot spots of N_2O emissions may depend on when in the growing season large rain events occur.

Although topographic depressions and rain events are generally considered major drivers of N_2O hot spots and hot moments, it is still challenging to predict much of the spatiotemporal variation in net soil-atmosphere N_2O emissions (Groffman et al., 2009). To better predict N_2O hot spots and hot moments, we suggest adopting a dynamic view of where hot spots and when hot moments of soil N_2O emissions occur as opposed to a static view of depressions such as hot spots and rain events as triggers for hot moments. To move toward this goal, we tested the following hypotheses: (1) the topographic index that best predicts spatial variation in N_2O emissions depends on recent rainfall amount, and (2) large rain events do not activate hot moments of N_2O fluxes under relatively cold temperatures that slow heterotrophic consumption of oxygen in soil pore water, even when soil inorganic N concentrations are not limiting. To test the first hypothesis, we measured N_2O emissions from 65 locations throughout an agricultural field before and after rain events over the course of a growing season, with a total of 11 sampling dates. To test the second hypothesis, we measured N_2O emissions, heterotrophic respiration rates, and soil O_2 concentrations in inundated soil cores under warm and cold conditions. The temperature treatments were also assessed in factorial combination with a nitrate treatment (ambient versus amended) to account for the role of nitrate limitation of denitrification in driving the observed soil N_2O emissions. This experiment was performed on intact soil cores collected from upslope and depressional areas of the field to assess if these areas of the field have different controls over soil N_2O emissions (i.e., to account for historical drainage legacy effects). Furthermore, the experiment was conducted both early and late in the growing season to account for effects of seasonal changes in microbial community composition.

2. Methods

2.1. Study Site

The study site was located at the University of Illinois at Urbana Champaign (UIUC) Energy Farm in Urbana, Illinois (40°03′58.9″N, 88°11′28.2″W). Specifically, the study took place in a 120 × 100 m field
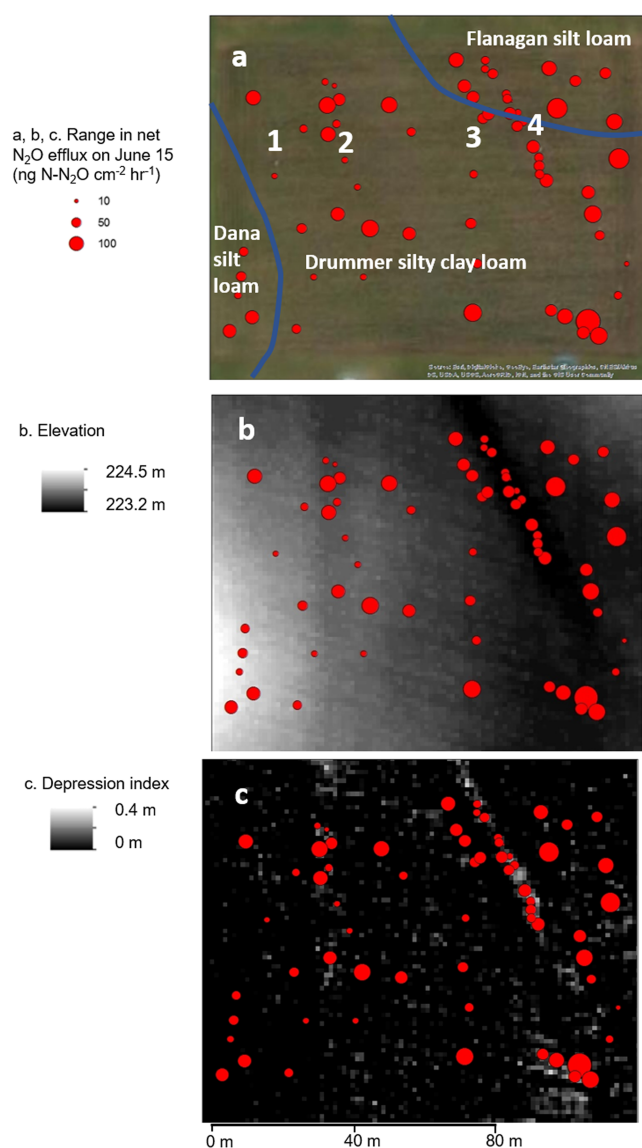
Figure 1. Soil series classifications (a), elevation (b), and localized depressions (c) of the 100 × 20 m study field in the UIUC Energy Farm. Scaled red dots represent magnitude of N$_2$O emissions from each of the 65 chambers on 15 June 2017, the day after a 32 mm rain event. The numbers indicate the locations where soil O$_2$ concentrations were measured within the field and correspond to the data in Figure 3.

that is managed under annual rotation between corn (*Zea mays*) and soybeans (*Glycine max*). The site is fertilized with 203 kg·N·ha^{-1} urea in the spring when *Z. mays* is planted, and it is not fertilized when *G. max* is planted. The field was planted with *G. max* during the 2017 growing season when this study took place. We chose to conduct this study in a field planted with *G. max* as *G. max* associates with nitrogen (N) fixing bacteria that can maintain higher soil inorganic N concentrations throughout the growing season compared with a single pulse of N fertilizer. Over the past 30 years, the mean annual precipitation was 1,045 mm, and the mean annual temperature was 10 °C at this site (Illinois climate network, 2017). During this time period, the average growing season (June–September) air temperature ranged 22–24 °C, and the mean April temperature averaged 11 °C (Illinois climate network, 2017).

2.2. Study Design

To capture spatial and temporal variability in soil GHG emissions, net soil-atmosphere fluxes of N$_2$O were measured 11 times from April 2017 through September 2017 from 65 sampling locations chosen to cover a range in soil series classifications and elevation found at the study site (Figure 1). These sampling dates included measurements the day after two large rain events in which over 30 mm of rain fell in a 24 hr period (on 1 May and 15 June) and after four smaller rain events (7 April, 17 April, 12 July, and 4 August). Surface ponding of soils was only observed following the 1 May rain event. LIDAR-derived topographic indices and soil series classifications were used to guide the selection of sampling locations. Sampling locations were chosen to span the elevation gradient in the field and to include areas that were identified as topographic depressions by the topographic fill model. Sampling locations were also chosen to span the different soil series present in the field, with the goal of covering spatial variability in soil properties relevant to soil drainage such as soil texture. There are three geographically associated soil series within the field that form a toposequence from upslope to depressional landform positions: Dana fine-silty soils, Flanagan silt loams, and Drummer silty clay loams. Soil series classifications were determined online using the Natural Resource and Conservation Service's Web Soil Survey tool (Soil Survey Staff, 2006).

2.3. Indices of Soil Drainage

LIDAR-derived topographic indices and magnetic susceptibility were used to identify areas likely to experience ponding following rain events. Elevation, latitude, and longitude of each sampling location was measured using a Trimble RTK GPS (Trimble, Sunnyvale, CA, USA) with accuracy of ±10 cm. Localized depression index was calculated using a hydraulic fill model based on a DTM derived from LIDAR data from the Illinois clearinghouse (Illinois State Geological Survey). This was done within ArcGIS v. 10.5 (ESRI, Redlands, CA, USA). Magnetic susceptibility was measured using a MS2 meter and MS2D loop attachment (Bartington Instruments Ltd, Oxon, England). Magnetic susceptibility is reported in dimensionless volume units (e.g., ×10^{-5}, SI units; Grimley et al., 2004).

2.4. Soil Characteristics

To characterize soil properties that may be drivers of soil N$_2$O emissions, soil organic C concentration, pH, bulk density, and texture were also measured from a soil sample collected at each gas flux sampling location at the end of the growing season. A 5 cm diameter by 10 cm depth soil core was taken from each location using a stainless steel soil corer (AMS, Inc., American Falls, ID, USA). The soil samples were weighed and

air dried in the laboratory prior to analyses. Soil organic C (SOC) concentrations were measured on ground soil samples using a Vario Micro Cube elemental analyzer (Elementar, Hanau, Germany). Bulk density was calculated as the dry soil weight divided by the volume of the core; the mass of rocks and organic matter were subtracted from the soil mass. The pH of each sample was measured in a 1:1 ratio of dry soil to deionized H_2O. Soil texture was measured using a hydrometer method (Gee & Bauder, 1986). Inorganic N concentrations were not measured as they vary greatly over short timescales (Krichels et al., 2019; Sebilo et al., 2013).

2.5. Soil Oxygen and Moisture Measurements

To determine how rain events affected surface and subsoil O_2 concentrations throughout the field, we monitored bulk soil O_2 and volumetric soil moisture concentrations at 10 and 20 cm depths quasicontinuously in the field. Bulk O_2 measurements measure O_2 concentrations in soil pore space and may not detect anaerobic microsites within soil aggregates (Sexstone, 1985). We installed Apogee SO-110 oxygen sensors fitted with AO-001 diffusion heads (Apogee Instruments, Logan, UT, USA) and CS655 soil moisture probes (Campbell Scientific, Logan, UT) at four locations within the field on 4 April 2017. To minimize soil disturbance during installation of the O_2 probes, we used a soil core to create a hole of a diameter matching that of the probes and of the desired sampling depth, gently inserted the probe into the hole, and repacked the hole with soil. To install the moisture probes, we dug a 30 cm deep hole adjacent to where the O_2 sensors were installed, inserted the probes horizontally into the undisturbed soil at 10 and 20 cm depth, and repacked the hole with soil. Only one of the four sampling locations was outfitted with moisture probes on 4 April, and the rest were installed on 7 May. The locations were chosen to cover the east to west elevation gradient across the field (Figure 1a). Voltage from the sensors was measured every minute, and 30 min averages were recorded on a CR-100 datalogger (Campbell Scientific, Logan, UT). Voltage measurements were converted to relative percent O_2 using a unique calibration factor for each probe empirically determined in the laboratory prior to field deployment. The probes were calibrated based on mV measurements at 0% O_2 (dinitrogen gas) and 20.95% O_2 (ambient air) in sealed jars containing water to create a humid environment. An empirical function provided in the Apogee SO-110 owner's manual was used to correct soil O_2 concentrations for temperature in the diffusion head as measured by the SO-110 sensor and atmospheric pressure measured at a nearby weather station (Illinois climate network, 2017). Sensors were removed from the field from 18 May through 1 June for planting of *G. max* and from 29 June through 2 July for application of pesticides. Data are also missing from three of the sensors starting 22 July due to battery failures.

2.6. Field Trace Gas Measurements

Net soil-atmosphere N_2O fluxes were measured manually using two-piece surface flux chambers. The chambers consisted of a 10 cm tall by 26 cm diameter vented acrylonitrile-butadiene-styrene chamber lid equipped with a rubber septum port and a vent placed on top of a PVC collar (Matson et al., 1990). The PVC collars were initially installed at each sampling location 1 week prior to the first sampling date on 7 April 2017. The collars were inserted 3–5 cm into the soil and were left in the field for the majority of the growing season. Collar height was measured on each sampling date, and the collars were inspected to ensure they were securely inserted into the soil. The collars had to be temporarily removed from 17 May through 1 June 2017 for planting of *G. max* and from 29 June through 2 July for the application of pesticides to the field. The collars were reinstalled within 10 cm of their original location as determined using a portable GPS (Trimble RTK). A 15 ml gas sample was collected from each chamber at 0, 10, 20, and 30 min after closing the lid. The gas samples were stored in 10 ml pre-evacuated glass vials sealed with thick rubber septa (Geo-Microbial Technologies, Inc., Ochelata, OK, USA) and aluminum crimps (Wheaton Industries Inc., Millville, NJ, USA). All flux measurements were performed between 10 a.m. and 3 p.m. to limit daily temperature changes; chambers were sampled in a different order each day to avoid systematic bias associated with sampling time. Additionally, air temperature within each chamber was measured to account for temperature effects on gas volume. After gas samples were collected, soil temperature and chamber temperature were measured using an Acorn Temp 5 meter (Oakton Instruments, Vernon Hills, IL, USA). All gas samples were analyzed on a Shimadzu GC-2014 (Shimadzu Scientific Instruments, Columbia, MD, USa) gas chromatograph (GC) equipped with an electron capture detector to measure concentrations of N_2O. Net N_2O fluxes were determined from the change in gas concentration over time using an iterative model that fits an exponential curve to the data (Matthias et al., 1978). Fluxes were recorded as zero when

there was no significant relationship between gas concentration and time ($p > 0.05$). Net fluxes from the field experiment are reported as mean $\pm$ standard deviation.

2.7. Laboratory Experimental Design

We carried out a lab experiment to test our hypothesis that cold temperatures inhibit N_2O emissions from inundated soils due to limited soil O_2 depletion by heterotrophic respiration. We sampled soils during the early and late growing season to determine if seasonal shifts in soil microbial community composition result in different response to temperature treatments. We also collected soils from a well-drained upslope portion of the field as well as from a poorly drained depressional portion of the field to determine if controls on soil N_2O emissions differ based on topographic position. Intact soil cores were flooded and subjected to experimental treatments to manipulate soil NO_3^- concentrations and temperature in a full factorial design ($n = 5$). The NO_3^- addition treatment was included to determine if soil N_2O emissions were limited by soil inorganic N concentrations rather than temperature, as *G. max* fields are not fertilized. Half of the soil cores were amended with enough NO_3^- to increase soil NO_3^- concentrations by 3.25 µg N-$NO_3 \cdot g^{-1}$ dry soil, which corresponds to typical soil NO_3^- concentrations during peak growing season when *Z. mays* is planted (Krichels et al. 2019). After flooding the intact soil cores, soil temperature was manipulated by placing half of the cores in a cold room that averaged 2 °C over the course of the experiment. The rest of the cores were kept at room temperature (22 °C). Net N_2O and CO_2 fluxes were measured from each core at 1, 2, and 5 days after flooding the cores. Soil O_2 concentrations at 5 cm depth were measured from a subset of the cores immediately prior to each N_2O and CO_2 flux measurement.

We collected 20 intact soil cores (0–10 cm depth) from an upslope and a depressional portion of the field (40 cores total) in March and in September using a 5 cm diameter soil corer fitted with a plastic sleeve for each soil core (AMS, Inc., American Falls, ID, USA). The soils were allowed to equilibrate on the benchtop in the laboratory for 2 days before the experimental treatments were initiated. The soil cores were flooded by injecting 10 ml of deionized water into each core using a spinal tap needle to evenly distribute the water vertically throughout the core. This was done four times such that at least 40 ml of added deionized water completely saturated the soils and left minimal (< 0.5 cm) standing water above the soil surface. If 40 ml of water did not saturate the core, then an additional 5–10 ml was added. For the late season experiment, 60 ml of water was needed to ensure complete saturation. For the NO_3^- addition treatment, a 1.02 mM KNO_3 solution in the initial 40 ml of DI used to flood the cores. The saturated soil cores were placed in quart-sized mason jars, which were left open but loosely covered with aluminum foil to keep the cores dark and to minimize water loss via evaporation. The intact cores were weighed daily to monitor water loss. All soils remained flooded for the duration of the experiment and no cores lost more than 1 ml of water over the course of the incubation.

To measure trace gas emissions from the soil cores, a 15 ml gas sample was collected from each jar immediately after sealing it with a lid equipped with butyl septum and again 4 hr later. Gas samples were stored in pre-evacuated 10 ml vials sealed with rubber septa and aluminum crimps (Wheaton Industries Inc., Millville, NJ, USA). Gas samples were analyzed on the GC as described earlier. Net trace gas fluxes were determined by calculating the linear change in jar headspace gas concentrations over the 4 hr incubation. A minimum detectable flux was calculated based on the standard deviation of three standard gas samples (1,001 ppm CO_2 and 1.08 ppm N_2O) run on the GC. The calculated detection limit for N_2O was 0.002 ppm$\cdot$hr^{-1} and for CO_2 was 2.4 ppm$\cdot$hr^{-1}. Net fluxes below this limit were considered not detectable and estimated as zero.

To measure soil O_2 concentrations, the intact soil cores were equipped with SP-PSt6-NAU Oxygen Sensor Spots (PreSens Precision Sensing, Regensburg, Germany). Each sensor spot was adhered to the inside of the soil core sleeve at 5 cm below the top of the core. These sensor spots measure gas and dissolved phase O_2 concentrations and are read using a fiber optic cable that can communicate with the spot through the plastic core (Fibox4 trace, PreSens Precision Sensing, Regensburg, Germany). Due to a limited number of sensor spots, only soil cores that did not receive the NO_3^- addition were equipped with a sensor spot, with only three replicates per treatment randomly selected for O_2 monitoring in the early growing season (12 cores total) and all five replicates per treatment monitored in the late growing season (20 cores total).

2.8. Statistics

All statistical analyses were performed using R version 3.5.2 (R Core Team, 2018). We used linear mixed effects models to determine the best predictors of soil N_2O flux on each sampling date. This was done using the lme function in the nlme package in R (Pinheiro et al., 2017). All N_2O flux data were assessed for normality with a Shapiro-Wilk test conducted using the stats package in R (R Core Team, 2018); log transformations were applied to normalize the data. When flux values below 1 ng $N-N_2O$ $cm^{-2} \cdot hr^{-1}$ occurred from a chamber for a given sampling date, a constant of 1 was added to flux values prior to log transformation. Elevation, localized depression index, percent clay, magnetic susceptibility, soil organic C concentrations, and pH were included as fixed independent variables in the initial model. We then used Akaike information criterion (AIC) to select which model terms to include in each model using the AIC package in R (R core team, 2018). We tested for the occurrence of spatial autocorrelation by calculating Moran's I using the ape package in R (Paradis & Schliep, 2018). If significant spatial autocorrelation was detected, then we corrected for it by adding a correlation matrix based on chamber distance from one another as a random effect to the model. Separate models were run for each sampling date. On some days many chambers did not exhibit significant N_2O emissions. However, we still ran our models on these days as hot spots can occur in part of the field even when other parts of the field have no detectable net soil-atmosphere N_2O fluxes. We ran an additional model using data from all 11 sampling days to elucidate which temporal variables best explained N_2O emissions from the entire field. For this model, soil temperature and total rainfall over the previous 48 hr were included as independent variables. Means and standard deviation are reported for elevation, localized depression index, percent clay, magnetic susceptibility, soil organic C concentrations, and pH. Relationships between these variables (R^2) were calculated using the lm function in R.

For the lab experiment, we ran mixed effects models to test for the effects of temperature, NO_3^-, and time since soil saturation on both N_2O emissions and CO_2 emissions from the intact soil cores. Separate models were run for soils collected early versus late in the growing season, as well as for soils collected from upslope versus depressional areas of the field. In each model, incubation temperature, NO_3^- addition, and sampling day were included as fixed variables, and core ID was included as a random variable. Core ID was included as a random variable to account for repeated measurements of the same cores over the course of the experiment. The models were run using the lme function in the nlme package in R (Pinheiro et al., 2017). We then used the anova.lme function from the nlme package to determine which factors best predicted both CO_2 and N_2O emissions. The same analyses were performed for soil O_2 concentrations. For the soil O_2 model, NO_3^- addition was not included as a factor as O_2 concentrations were not measured from the cores that received NO_3^- addition.

3. Results

3.1. Soil Drainage Variables

The study field exhibited a microtopographic gradient, ranging from 223.6 m above sea level at the highest point to 222.6 m above sea level at the lowest (Figure 1). The topographic fill model showed that 30 of the 65 sampling locations were located in topographic depressions, which averaged 0.12 m in depth relative to the immediate surrounding terrain. None of these topographic depressions were located on Dana soils, which are the most elevated soil series in the toposequence at the site, but they were evenly distributed between Flanagan and Drummer soils (Figure 1b). Magnetic susceptibility averaged $19.6 \times 10^{-5} \pm 12.1 \times 10^{-5}$ SI units ($\pm$ standard deviation; Table 1) and was positively correlated with elevation ($R^2 = 0.66$, $p < 0.001$, $n = 65$; Table 2).

Soil clay content, SOC concentrations, and pH varied considerably within the field (Table 1). Soil clay content averaged $24.9 \pm 4.82\%$ and ranged 15.2–34.3%. Soil organic C averaged $2.30 \pm 0.22\%$ and ranged 1.88–2.72% throughout the field. Soil bulk density ranged 1.09–1.50 $g \cdot cm^{-3}$, while soil pH ranged 5.45–7.17. Soil organic carbon concentration and clay content were negatively correlated with elevation (SOC: $R^2 = 0.38$, $p < 0.001$, $n = 65$; clay: $R^2 = 0.56$, $p < 0.001$, $n = 65$), while soil pH exhibited a weak positive correlation with elevation ($R^2 = 0.04$, $p < 0.05$, $n = 65$, Table 2). Soil organic carbon concentration and clay content were also significantly positively correlated ($R^2 = 0.42$, $p < 0.001$, $n = 65$, Table 2).

Table 1

Mean, Standard Deviation, Minimum, and Maximum of Soil Properties Across 65 Sampling Locations Within the Study Field

Soil property	Mean	Standard deviation	Minimum	Maximum
Elevation (masl)	222.6	0.30	222.3	223.6
Magnetic susceptibility	19.6	12.1	11.1	69.1
Soil organic C concentration (%)	2.30	0.22	1.88	2.72
Clay content (%)	24.9	4.82	15.2	34.3
Bulk density (g dry soil cm^{-3})	1.30	0.08	1.09	1.50

3.2. Rainfall, Soil O_2 Concentrations, and Soil Moisture

While cumulative precipitation between April and September 2017 was comparable to the previous five growing seasons (Figure 2), a greater proportion of this rainfall occurred early in the growing season. Between 1 April and 1 June 2017, 300 mm of rain fell, compared with an average of 225 ± 34 mm during this same time in 2012 through 2016 (Figure 2). However, only 177 mm of rain fell between 1 June and 1 September 2017, compared with an average of 337 ± 51 mm during this time frame in 2012 through 2016 (Figure 2).

In situ soil gas phase O_2 concentrations in all four locations in the field decreased in response to large rain events in the early to middle growing season (Figure 3). After a 37.1 mm rain event on 1 May, soil O_2 concentrations fell to 5–15% throughout the field at both 10 and 20 cm depths, while volumetric soil moisture reached 45%. After a 32 mm rain event on 14 June, soil O_2 remained above 12% at 10 cm depth throughout the field and dropped to 0% at 20 cm depth in some parts of the field. Soil moisture at 10 and 20 cm depth increased by 5–10% following this rain event (Figures 3d and 3e). For the rest of the growing season (through the end of September), soil O_2 concentrations at both soil depths remained close to atmospheric concentrations, despite moderate rain events and one large rain event (32 mm on 28 August) that occurred after 15 June (Figure 3a). During this time, soil moisture ranged between 25% and 38% throughout the field and increased by approximately 3% following the large rain event on 28 August.

3.3. Field N_2O Emissions

The highest N_2O emissions were observed on 15 June, after a 32 mm rain event the previous day (Figures 4a and 4b). On this date, N_2O emissions averaged 66.5 ± 42.6 ng N-$N_2O \cdot cm^{-2} \cdot hr^{-1}$ ($\pm$ standard deviation) from the 65 chambers. There was significant spatial autocorrelation in N_2O flux (Moran's I, $p < 0.05$; Table 2). The mixed model explained 18% of the variation in N_2O emissions on this date, with elevation, depression index, magnetic susceptibility, and pH as significant model terms (Table 3). Magnetic susceptibility was positively correlated with N_2O emissions, while the rest of the model terms were negatively correlated with N_2O emissions (Table 3).

The only other sampling date when all 65 chambers had significant N_2O emissions was on 12 July, the day after a 24.4 mm rain event, when emissions averaged 10.4 ± 10.1 ng N-$N_2O \cdot cm^{-2} \cdot hr^{-1}$. There was no significant spatial autocorrelation in N_2O emissions on this day (Moran's I, $p = 0.09$). The soil drainage model explained only 9% of the variation in N_2O emissions, with magnetic susceptibility and pH as the only two terms selected for the model. Magnetic susceptibility was positively correlated with N_2O emissions, and pH was negatively correlated with N_2O emissions (Table 3).

The models explained the most variation in N_2O emissions on 10 August ($R^2 = 0.29$) and 17 September ($R^2 = 0.28$) when no rainfall had fallen in the previous 48 hr. On 10 August, N_2O emissions averaged 2.24 ± 3.41 ng N-$N_2O \cdot cm^{-2} \cdot hr^{-1}$, and 39 of the 65 sampling locations had significant N_2O emissions (Figure 4). On this date, elevation and pH were both significant terms in the model ($p < 0.05$) and were negatively correlated with N_2O emissions (Table 3). On 17 September, N_2O emissions averaged 2.81 ± 3.09 ng N-$N_2O \cdot cm^{-2} \cdot hr^{-1}$, and 49 of the 65 sampling locations had

Table 2

Coefficient of Determination (R^2) Between All Measured Soil Properties as Determined Using Linear Models

Soil property	Depression	Clay	MS	SOC	pH
Elevation	**0.16**	**0.56**	**0.66**	**0.38**	**0.04**
Depression		**0.11**	0.07	0.04	**0.06**
Clay			**0.22**	**0.42**	0.01
MS				**0.10**	0.03
SOC					**0.05**

Note. Bold values indicate significant correlation at $p < 0.05$.
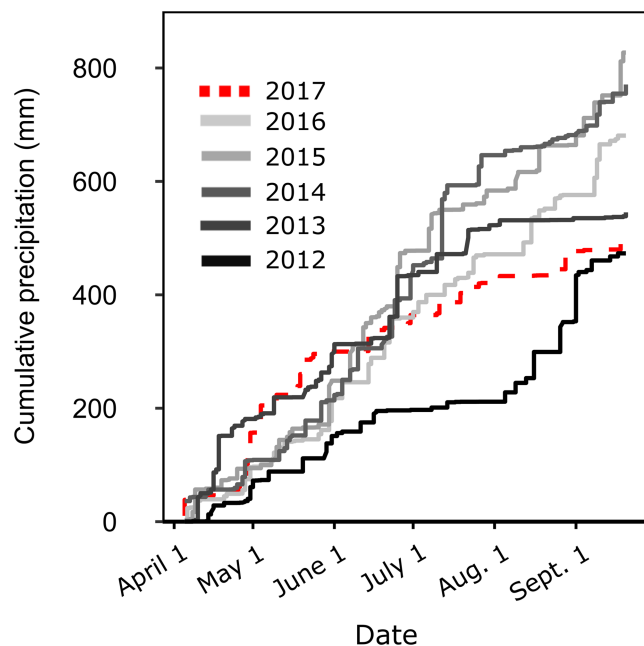
Figure 2. Cumulative precipitation during the 2012–2017 growing seasons (1 April through 15 September). The red line represents the 2017 growing season when this study was conducted, and black through lighter gray lines represent 2012 through 2016.

significant N_2O emissions (Figure 4). On this date, topographic depression index and SOC concentration were the only significant terms in the model ($p < 0.05$, Table 2), with both negatively correlated with N_2O emissions. During the first five sampling dates (7 April through 7 June), N_2O emissions averaged less than 1.0 ng $N-N_2O$ $cm^{-2} \cdot hr^{-1}$ on each day (Figure 4b), and 30–58 of the chambers did not exhibit detectable N_2O fluxes.

Much of the temporal variation in soil N_2O could be explained by the interaction between soil temperature and how much rain had fallen in the previous 48 hr ($R^2 = 0.69$, $p < 0.001$).

3.4. Laboratory Experiment

Early in the growing season, there was a significant interactive effect of temperature and day of experiment on soil O_2 concentrations, CO_2 emissions, and N_2O emissions from both upslope and depressional soils (Figure 5). Soil O_2 concentrations remained below 4% in soils incubated at room temperature (Figures 5a and 5d). In contrast, O_2 concentrations in soils incubated at 2 °C decreased slowly over the course of the incubation, from $10.9 \pm 0.87\%$ to $2.7 \pm 0.90\%$ in upslope soils (temperature * day of experiment interaction: $F_{2,10} = 4.27$, $p < 0.05$; Figure 5a) and from $13.6\% \pm 0.91\%$ to 3.8 ± 1.0 in depressional soils (temperature * day of experiment interaction: $F_{2,10} = 18.2$, $p < 0.001$; Figure 5d). Carbon dioxide emissions were consistently higher from soils incubated at 22 °C and increased over time in both temperature treatments (Figures 5b and 5e). This pattern was observed for upslope soils (temperature * day of experiment interaction: $F_{2,32} = 11.1$, $p < 0.001$; Figure 5b) and depressional soils (temperature * day of experiment interaction: $F_{2,32} = 5.36$, $p = 0.01$; Figure 5e). Nitrous oxide emissions from upslope soils were initially greater from soils incubated at 22 °C (0.93 ± 0.16 ng $N \cdot g^{-1} \cdot hr^{-1}$) compared with soils incubated at 2 °C (-0.01 ± 0.01 ng $N \cdot g^{-1} \cdot hr^{-1}$; Figure 5c). However, after remaining flooded for four days, this pattern reversed. In upslope soils, N_2O emissions decreased to 0.01 ± 0.01 ng $N \cdot g^{-1} \cdot hr^{-1}$ at 22 °C and increased to 0.86 ± 0.58 ng $N \cdot g^{-1} \cdot hr^{-1}$ at 2 °C (temperature * day of experiment interaction: $F_{2,32} = 10.4$, $p < 0.001$). Nitrous oxide emissions from depressional soils incubated at 22 °C also decreased over time, but N_2O emissions from depressional soils incubated at 2 °C were more variable, and no obvious temporal pattern was observed (temperature * day of experiment interaction: $F_{2,32} = 3.98$, $p = 0.03$; Figure 5f).

Late in the growing season, temperature effects and temporal patterns in soil O_2 concentrations and CO_2 emissions mimicked what was observed early in the growing season from both upslope and depressional soils (Figure 6). However, patterns in soil N_2O emissions from upslope soils differed between sampling dates. Specifically, N_2O emissions were highest from warm NO_3^- amended upslope soils late in the growing season (temperature * NO_3^- addition interaction: $F_{1,16} = 6.54$, $p = 0.02$; Figure 6c), which was not exhibited in the early season. Soil N_2O emissions from upslope soils incubated at 22 °C remained higher than N_2O emissions from cold-treated soils for the entire late season experiment (Figure 6c). Additionally, the NO_3^- amended upslope soils incubated at 22 °C had higher N_2O emissions compared with the ambient NO_3^- soils incubated at 22 °C throughout the late season experiment. In contrast, NO_3^- addition did not affect N_2O emissions from depressional soils during the late growing season ($F_{1,16} = 2.3$, $p = 0.15$). However, there was a significant interaction effect between temperature and day of experiment on N_2O emissions from depressional soils late in the growing season ($F_{2,32} = 15.4$, $p < 0.001$; Figure 6f), as was observed from both upslope and depressional soils early in the early growing season (Figures 5c and 5f).

4. Discussion

Contrary to the static view of rainfall events as triggers of N_2O hot moments and topographic depressions as N_2O hot spots, our data show that hot moments of N_2O emissions do not always occur after large rain events and microtopographic depressions do not necessarily determine where hot spots of N_2O emissions develop. Pulses in soil N_2O emissions were only observed after one large rain event in June and not after rainfall in
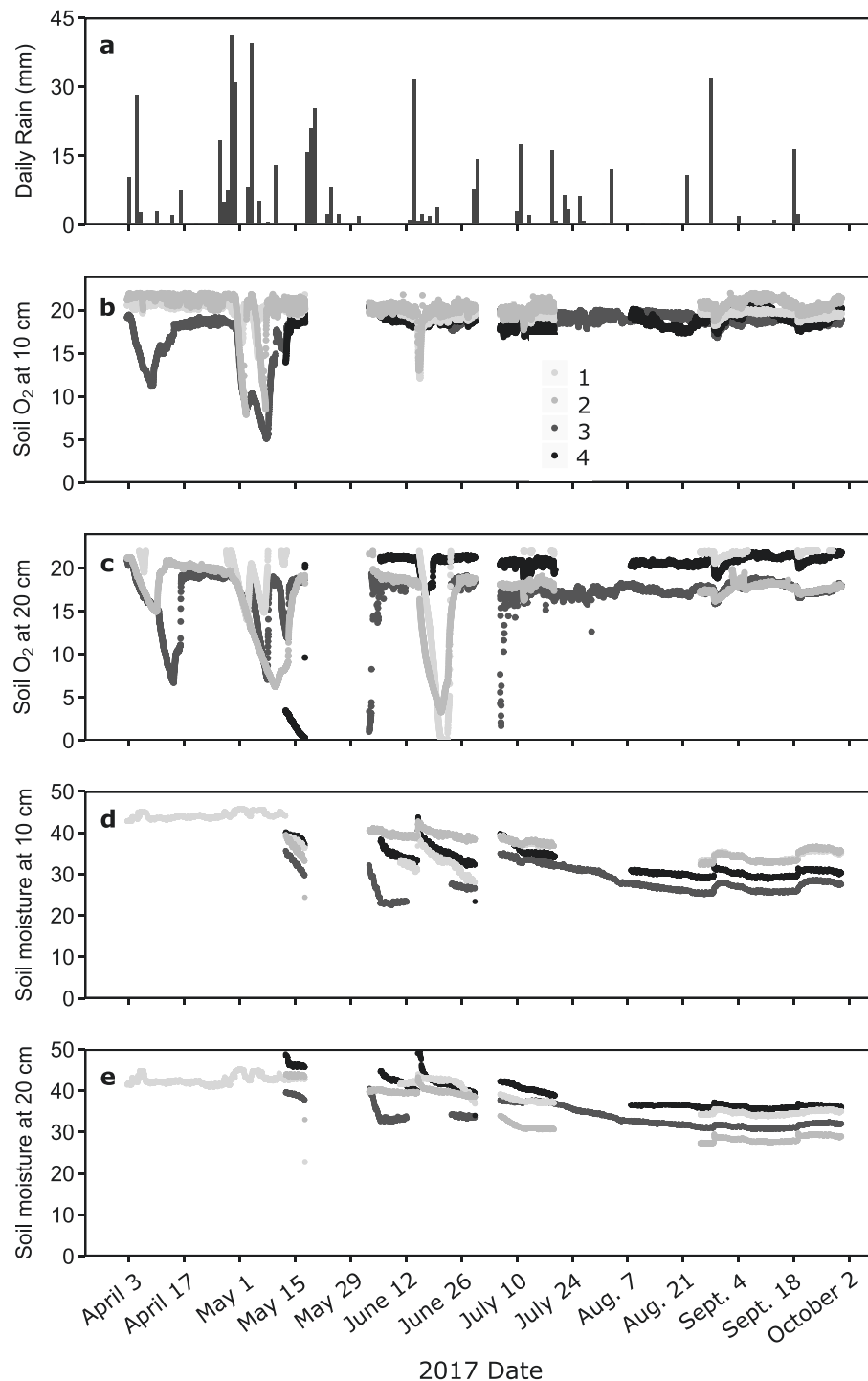
Figure 3. Daily precipitation (mm; a), soil O_2 concentration (%) at 10 cm depth (b), soil O_2 concentration at 20 cm depth (c), volumetric soil moisture (%) at 10 cm depth (d), and volumetric soil moisture at 20 cm depth (e). Different colors represent different sensor locations within the field as shown in Figure 1a. The numbers correspond to the locations shown in Figure 1a. Sensors were removed from the field from 18 May through 1 June for planting of *G. max* and from 29 June through 2 July for application of pesticides. Data are also missing from three of the sensors starting 22 July due to battery failures.

the early spring and late summer. Results from the lab experiment suggest that cold temperatures prevent the depletion of soil O_2 concentrations by microbial respiration following large rainfall in the spring, delaying the onset of denitrification. Late in the growing season, high plant evapotranspiration rates may prevent large rain events from saturating soils and establishing anoxic conditions necessary for N_2O
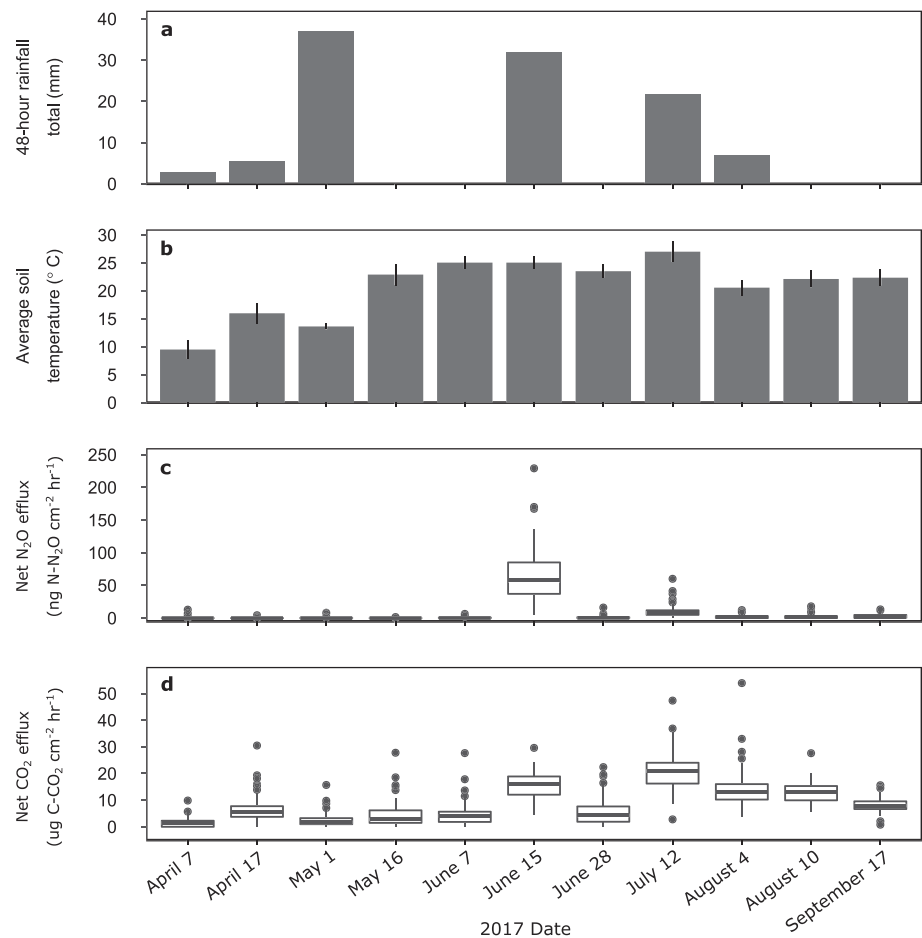
Figure 4. Total rainfall over the 48 hr prior to trace gas measurements (a), mean soil temperature ± standard deviation (b), mean N_2O emissions (c), and CO_2 emissions (d) as measured on 11 days over the course of the 2017 growing season. The line in each box in panels c and d represents the mean ($n = 65$), the upper and lower portions of each box correspond to the 25th and 75th percentiles, the whiskers extend to the upper and lower interquartile range, and dots represent outliers.

Table 3
Summary of Statistical Results From Soil Drainage Linear Mixed Effects Models of N_2O Emissions on Each Sampling Date

Date	Elevation	Depression	Clay	MS	SOC	pH	R^2	Moran's I
7 April	**−0.38**	–	**−0.06**	**0.02**	0.63	—	0.22	0.11
17 April	—	—	—	—	—	—	0.00	0.39
1 May	**0.14**	—	—	**−0.01**	—	—	0.09	0.20
16 May	0.04	—	0.01	—	—	—	0.05	0.79
7 June	**0.29**	—	—	**−0.02**	—	−1.7	0.16	<0.01
15 June	**−0.34**	**−0.36**	—	**0.02**	—	**−3.7**	0.18	0.03
28 June	—	—	**−0.04**	—	—	—	0.08	0.83
12 July	—	—	—	**−0.01**	—	2.9	0.09	0.09
4 August	**0.61**	**−0.04**	—	—	**1.89**	—	0.19	<0.01
10 August	**−0.41**	—	—	**0.02**	—	**−5.1**	0.29	<0.01
17 September	—	**−0.43**	—	—	**−0.87**	—	0.28	<0.01

Note. The dependent variable in this model was log(N_2O emissions + 1), and the independent variables were elevation, depression index, clay content, magnetic susceptibility (MS), soil organic C concentration (SOC), and pH. AIC selection criteria were used to select model terms; only the selected terms are reported for each model. The coefficient for each model term is presented; coefficients for statistically significant model terms ($p < 0.05$) are in bold. The total R^2 for each model is also presented. When spatial autocorrelation was detected (Moran's $I < 0.05$), the model included a gaussian error term to account for this. The p value for Moran's I is also reported.
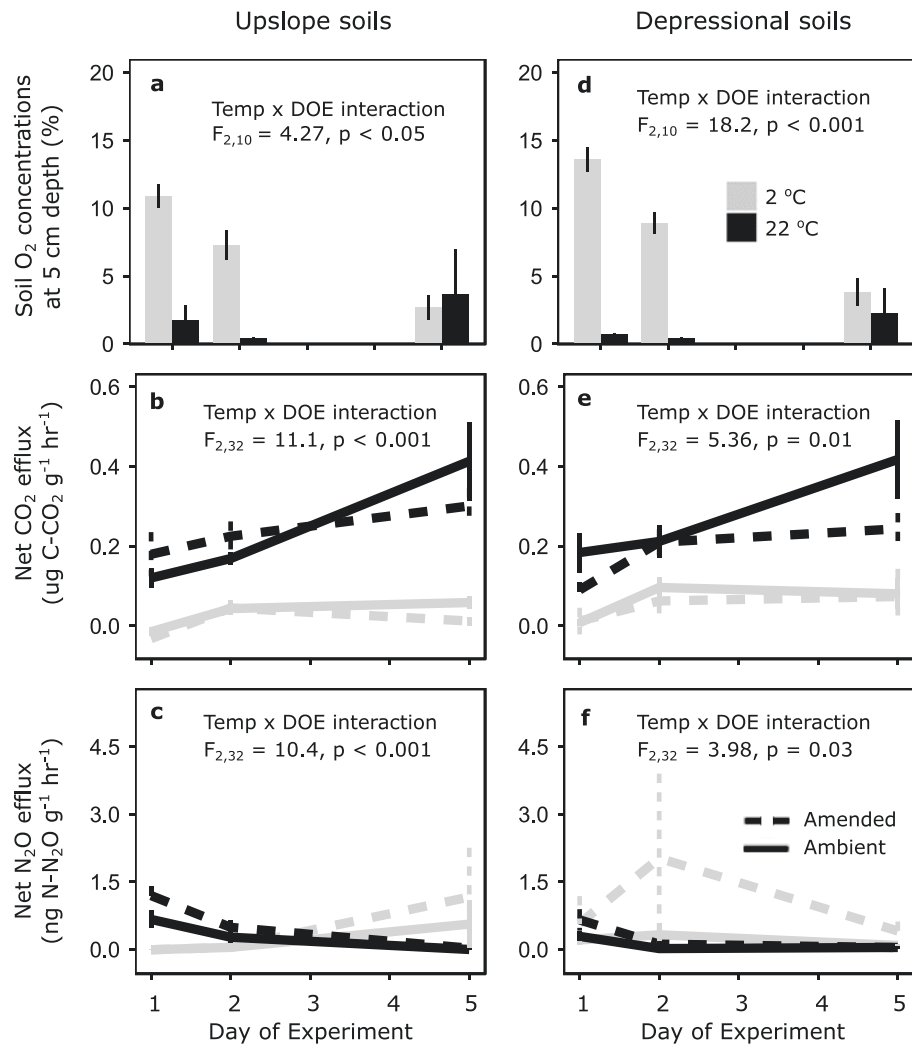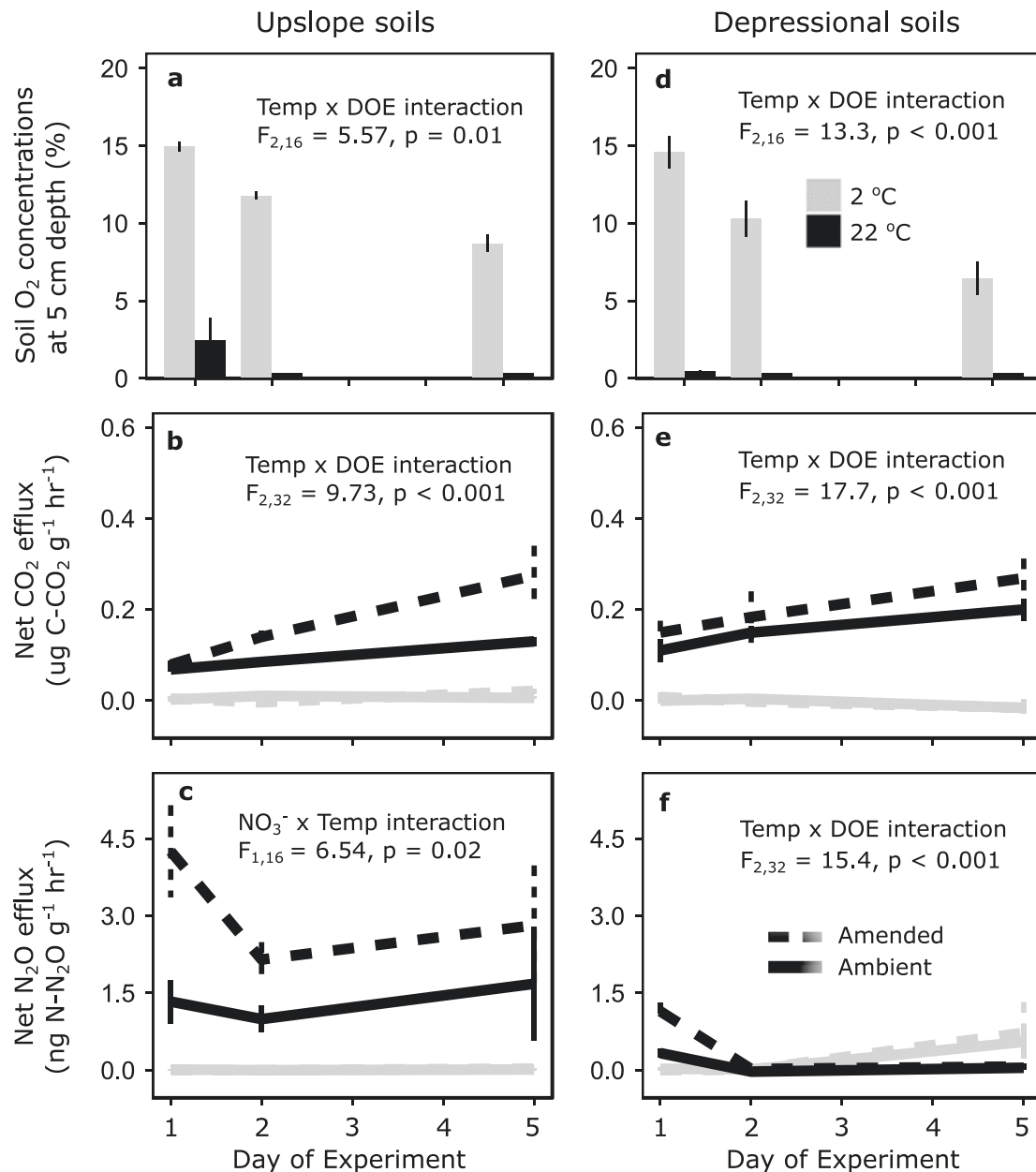
Figure 5. Soil O_2 concentration at 5 cm depth (a, d), CO_2 emissions (b, e), and N_2O emissions (c, f) from intact soil cores for the lab incubation experiment conducted early in the growing season ($n = 3$ for a and d, $n = 5$ for b, c, e, and f). Error bars represent standard errors. Data for soils collected from an upslope portion of the field (a, b, c) and a depressional portion of the field (d, e, f) are shown separately. Gray lines correspond to soils incubated at 2 °C, while black lines correspond to soils incubated at 22 °C. Dashed lines represent soils amended with NO_3^-, and solid lines represent ambient NO_3^- concentrations.

production via denitrification. When significant N_2O emissions were measured, models including various proxies for microtopography did not explain much of the spatial variation in N_2O emissions. This may be a result of other controls over soil moisture, such as evapotranspiration, preventing spatial patterns in soil O_2 concentrations. We also show that soil drainage legacy effects can develop over the course of the growing season and that this may obscure any spatial patterns in soil N_2O emissions associated with topographic variation at the field scale. Below, we explore possible mechanisms driving these patterns and what consequences they might have for predicting N_2O emissions in response to climate change.

We hypothesized that different indices of microtopography would best predict field-scale variation in soil N_2O emissions based on recent rainfall amounts but found that all indices we examined were weak predictors. While different topographic indices were significant model terms on each sampling date, no model explained more that 29% of the spatial variation in soil N_2O emissions on any given day (Table 3). This contrasts with prior observations that poorly drained topographic depressions consistently act as hot spots of soil N_2O emissions (Turner et al., 2016; Velthof et al., 1996; Yanai et al., 2003). However, these studies targeted measurements after fertilization that could have led to NO_3^- accumulation in depressions

Figure 6. Soil O_2 concentration at 5 cm depth (a, d), CO_2 emissions (b, e), and N_2O emissions (c, f) from intact soil cores for the lab incubation experiment conducted late in the growing season ($n = 5$). Error bars represent standard errors. Data for soils collected from an upslope portion of the field (a, b, c) and a depressional portion of the field (d, e, f) are shown separately. Gray lines correspond to soils incubated at 2 °C, while black lines correspond to soils incubated at 22 °C. Dashed lines represent soils amended with NO_3^-, and solid lines represent ambient NO_3^- concentrations.

to create the N_2O hot spots, whereas we intentionally conducted our study in unfertilized *G. max* field to isolate the effects of rainfall and topography on soil N_2O emissions. The field-scale patterns in soil N_2O emissions over the growing season suggest other variables not directly related to microtopography could be more important in explaining spatial variation in soil N_2O emissions. For example, during peak growing season, high evapotranspiration rates from crops can draw large amounts of water out of soils (Sophocleous, 2002), helping retain oxic conditions that prevent denitrification from taking place (Knowles, 1982). As such, at peak plant biomass, high evapotranspiration rates may prevent depressional areas from experiencing hypoxic conditions necessary to drive spatial patterns in N_2O emissions. Moreover, spatial variation in other soil properties such as microbial community composition (Philippot et al., 2009) or soil structure (Palta et al., 2016) may contribute to field-scale patterns in soil N_2O

emissions. This may explain why our models, which did not include these variables, only explained up to 18% of the variation in soil N_2O emissions after a large rain event in mid-June when emissions were the most variable across the field. Although our data did not support our hypothesis, they do suggest that the controls on spatial variation in soil N_2O emissions likely change over the course of the growing season and that topographic indices alone are insufficient to predict much of this variation.

The development of historical soil drainage legacy effects over the growing season can make it difficult to use microtopographic indices to predict the location of hot spots of N_2O emissions. When upslope and depressional soils were incubated under the same inundated and warm conditions late in the growing season, the upslope soils exhibited higher N_2O emissions compared with the depressional soils (Figure 6c). This laboratory observation of a soil drainage legacy effect is consistent with patterns in soil N_2O emissions documented in a nearby field after large rain events that caused ponding in the middle to late growing season (Krichels et al., 2019). However, the soil drainage legacy effect was not manifested in the early growing season laboratory experiment (Figure 5c), suggesting that upslope and depressional soils have different controls over N_2O dynamics that are established over the course of the growing season. For example, upslope and depressional soils can have distinct denitrifying microbial communities (Suriyavirun et al., 2019), and the active community composition may further diverge over the course of the growing season as a result of differences in soil O_2 fluctuations (DeAngelis et al., 2010; Krichels et al. ,2019) or plant-microbe interactions (Buyer et al., 2002; Mbuthia et al., 2015). Furthermore, differences in soil structure between upslope and depressional soils can alter the distribution of water and O_2 in soil pores (Algayer et al., 2014; Askaer et al., 2010; Sey et al., 2008), thus affecting soil denitrification rates (Krichels et al., 2019; Palta et al., 2016). Changes in soil structure can occur over the course of the growing season as a result of variable water fluctuations (De-Campos et al., 2009; Horn & Smucker, 2005; Six et al., 2004) and may be homogenized following annual tillage of agricultural fields (Six et al., 2004). As such, historical soils drainage legacy effects can be established over the course of the growing season, contributing to the dynamic nature of hot spots and hot moments of N_2O emissions.

Although precipitation is often associated with hot moments of soil N_2O emissions (Dobbie & Smith, 2003; Li et al., 1992; Sexstone et al., 1985), we found that hot moments only occurred following large rain events during the middle of the growing season (Figure 4). Heavy rainfall stimulated the highest N_2O emissions observed in this study during warm conditions in mid-June, but rain events of similar magnitude failed to stimulate hot moments in N_2O emissions under cool conditions early in the growing season. In the laboratory, microbial respiration in cold soils was significantly lower than in warm soils and took multiple days to consume enough O_2 to induce denitrification (Figures 5 and 6), supporting our hypothesis that low temperatures can indirectly inhibit denitrification. Temperature limitation of N_2O emissions occurred even when NO_3^- was added to soil incubations in the lab, suggesting that low N_2O emissions observed in the field during the cool spring may not have been due to NO_3^- limitation in unfertilized *G. max* fields. While the laboratory treatment was colder than spring soil temperatures in the field, cool soil temperatures in the field could still slow microbial respiration enough to delay the onset of hypoxic conditions for over 24 hr following rainfall, the timescale at which our field measurements were conducted. Assuming that rates of microbial respiration are twice as high at 12 °C compared with 2 °C ($Q_{10} = 2$; Meyer et al., 2018) and that this doubles the rate of O_2 consumption compared with rates observed under cold conditions in the lab, it would take 47 hr for microbial respiration to establish anaerobic conditions at 12 °C. Higher O_2 concentrations in cold incubated soils were not just a result of increased solubility of O_2 in cold water (Han & Bartels, 1996), as the low respiration rates under cold conditions still decreased dissolved O_2 concentrations over the 4 day incubation. While low temperatures can directly inhibit denitrification enzyme activity (Braker et al., 2010; Holtan-Hartwig et al., 2002), N_2O emissions from soils increased after 4 days of flooding under cold conditions. This increase was concomitant with a decline in soil O_2 concentrations, suggesting that the presence of O_2 rather than direct temperature limitation on denitrifier activity suppressed N_2O emissions under cold conditions. Ponding of depressional areas typically only lasts 1–2 days following large rainfall (Krichels et al., 2019), which may not be long enough to stimulate denitrification under cold conditions. An alternative explanation to N_2O hot moments occurring only in the summer is that interludes between rain events were longer (up to 18 days) in the summer than in the spring, potentially leading to the Birch effect driving trace gas emissions by releasing labile C upon wetting of the soil (Birch, 1958). However, the mesic soils in our study remained above 20% volumetric soil moisture (Figures 3d and 3e) and therefore did not dry to the same extent observed during the months-long dry season in Mediterranean

ecosystems where the Birch effect plays an important role (Austin et al., 2004). Taken together, these results suggest that the development of N_2O hot spots following spring rainfall can be delayed if cool temperatures constrain O_2 consumption in soil pore water.

In conclusion, we show that the controls on the location and timing of hot spots and hot moments of N_2O emissions are dynamic over the course of the growing season. Microtopographic depressions did not consistently act as hot spots of N_2O emissions, and large rain events only triggered hot moments of N_2O emissions under warm conditions during peak growing season. Seasonal changes in temperature, crop growth, and soil microbial community composition may mediate the effects of topography and rainfall on soil N_2O emissions, leading to dynamic controls on the formation of N_2O hot spots and hot moments. Global climate models predict that a greater proportion of cumulative annual rainfall will occur in spring instead of summer months, resulting in wetter springs and drier summers (USGCRP 2009; Min et al., 2011). Changes in soil greenhouse gas emissions in response to changing precipitation regimes have the potential to feedback on climate change. Our findings suggest that cool temperatures may constrain N_2O hot moments in response to spring precipitation and that shallow topographic depressions may not harbor N_2O hot spots during drier summer months. This suggests that increased frequency and magnitude of precipitation events may not necessarily increase soil N_2O emissions to have a positive feedback on climate change. Moving beyond a static view of depressions and large rain events as triggers for N_2O hot spots and hot moments could allow us to better predict ecosystem scale changes in soil N_2O emissions resulting from changing precipitation regimes.

References

Algayer, B., Le Bissonnais, Y., & Darboux, F. (2014). Short-term dynamics of soil aggregate stability in the field. *Soil Science Society of America Journal*, *78*(4), 1168–1176. https://doi.org/10.2136/sssaj2014.01.0009

Ambus, P., & Christensen, S. (1994). Measurement of N_2O emission from a fertilized grassland: An analysis of spatial variability. *Journal of Geophysical Research*, *99*(D8), 16549. https://doi.org/10.1029/94JD00267

Andrews, J. A., Matamala, R., Westover, K. M., & Schlesinger, W. H. (2000). Temperature effects on the diversity of soil heterotrophs and the $\delta^{13}C$ of soil-respired CO_2. *Soil Biology and Biochemistry*, *32*(5), 699–706. https://doi.org/10.1016/S0038-0717(99)00206-0

Askaer, L., Elberling, B., Glud, R. N., Kühl, M., Lauritsen, F. R., & Joensen, H. P. (2010). Soil heterogeneity effects on O_2 distribution and CH_4 emissions from wetlands: In situ and mesocosm studies with planar O_2 optodes and membrane inlet mass spectrometry. *Soil Biology and Biochemistry*, *42*(12), 2254–2265. https://doi.org/10.1016/j.soilbio.2010.08.026

Austin, A. T., Yahdjian, L., Stark, J. M., Belnap, J., Porporato, A., Norton, U., et al. (2004). Water pulses and biogeochemical cycles in arid and semiarid ecosystems. *Oecologia*, *141*(2), 221–235. https://doi.org/10.1007/s00442-004-1519-1

Baldwin, D. S., & Mitchell, A. M. (2000). The effects of drying and re-flooding on the sediment and soil nutrient dynamics of lowland river–floodplain systems: A synthesis. *Regulated Rivers: Research & Management*, *16*(5), 457–467. https://doi.org/10.1002/1099-1646(200009/10)16:5<457::aid-rrr597>3.3.co;2-2

Bernhardt, E. S., Blaszczak, J. R., Ficken, C. D., Fork, M. L., Kaiser, K. E., & Seybold, E. C. (2017). Control points in ecosystems: moving beyond the hot spot hot moment concept. *Ecosystems*, *20*(4), 1–18. https://doi.org/10.1007/s10021-016-0103-y

Birch, H. F. (1958). The effect of soil drying on humus decomposition and nitrogen availability. *Plant and Soil*, *10*(1), 9–31. https://doi.org/10.1007/BF01343734

Bradford, M. A., Davies, C. A., Frey, S. D., Maddox, T. R., Melillo, J. M., Mohan, J. E., et al. (2008). Thermal adaptation of soil microbial respiration to elevated temperature. *Ecology Letters*, *11*(12), 1316–1327. https://doi.org/10.1111/j.1461-0248.2008.01251.x

Braker, G., Schwarz, J., & Conrad, R. (2010). Influence of temperature on the composition and activity of denitrifying soil communities. *FEMS Microbiology Ecology*, *73*(1), 134–148. https://doi.org/10.1111/j.1574-6941.2010.00884.x

Burke, I. C., Yonker, C. M., Parton, W. J., Cole, C. V., Schimel, D. S., & Flach, K. (1989). Texture, climate, and cultivation effects on soil organic matter content in U.S. grassland soils. *Soil Science Society of America Journal*, *53*(3), 800. https://doi.org/10.2136/sssaj1989.03615995005300030029x

Buyer, J. S., Roberts, D. P., & Russek-Cohen, E. (2002). Soil and plant effects on microbial community structure. *Canadian Journal of Microbiology*, *48*(11), 955–964. https://doi.org/10.1139/w02-095

Ciais, P., Sabine, C., Bala, G., Bopp, L., Brovkin, V., Canadell, J., et al. (2013). Carbon and other biogeochemical cycles. *Climate Change 2013 - The Physical Science Basis*, 465–570. https://doi.org/10.1017/CBO9781107415324.015

Chapuis-Lardy, L., Wrage, N., Metay, A., Chotte, J.-L., & Bernoux, M. (2007). Soils, a sink for N_2O? A review. *Global Change Biology*, *13*(1), 1–17. https://doi.org/10.1111/j.1365-2486.2006.01280.x

Davidson, E. A., Samanta, S., Caramori, S. S., & Savage, K. (2012). The Dual Arrhenius and Michaelis-Menten kinetics model for decomposition of soil organic matter at hourly to seasonal time scales. *Global Change Biology*, *18*, 371–384. https://doi.org/10.1111/j.1365-2486.2011.02546.x

De-Campos, A. B., Mamedov, A. I., & Huang, C. (2009). Short-term reducing conditions decrease soil aggregation. *Soil Science Society of America Journal*, *73*(2), 550–559. https://doi.org/10.2136/sssaj2007.0425

De-Campos, A. B., Huang, C. H., & Johnston, C. T. (2012). Biogeochemistry of terrestrial soils as influenced by short-term flooding. *Biogeochemistry*, *111*(1-3), 239–252. https://doi.org/10.1007/s10533-011-9639-2

DeAngelis, K. M., Silver, W. L., Thompson, A. W., & Firestone, M. K. (2010). Microbial communities acclimate to recurring changes in soil redox potential status. *Environmental Microbiology*, *12*(12), 3137–3149. https://doi.org/10.1111/j.1462-2920.2010.02286.x

Dobbie, K. E., & Smith, K. A. (2003). Nitrous oxide emission factors for agricultural soils in Great Britain: The impact of soil water-filled pore space and other controlling variables. *Global Change Biology*, *9*(2), 204–218. https://doi.org/10.1046/j.1365-2486.2003.00563.x

Estop-Aragonés, C., Knorr, K. H., & Blodau, C. (2013). Belowground in situ redox dynamics and methanogenesis recovery in a degraded fen during dry-wet cycles and flooding. *Biogeosciences*, *10*, 421–436. https://doi.org/10.5194/bg-10-421-2013

Fink, C. M., & Drohan, P. J. (2016). High resolution hydric soil mapping using LiDAR digital terrain modeling. *Soil Science Society of America Journal*, *0*(0), 0. https://doi.org/10.2136/sssaj2015.07.0270

Fissore, C., Dalzell, B. J., Berhe, A. A., Voegtle, M., Evans, M., & Wu, A. (2017). Influence of topography on soil organic carbon dynamics in a Southern California grassland. *Catena*, *149*, 140–149. https://doi.org/10.1016/j.catena.2016.09.016

Gee, G. W., & Bauder, J. W. (1986). Particle-size analysis. In A. Klute (Ed.), *Methods of soil analysis. Part 1. Physical and mineralogical methods* (second, Vol. 9, pp. 383–411). Madison, WI: American Society of Agronomy, Soil Science Society of America.

Goodroad, L. L., & Keeney, D. R. (1984). Nitrous oxide production in aerobic soils under varying pH, temperature and water content. *Soil Biology and Biochemistry*, *16*(1), 39–43. https://doi.org/10.1016/0038-0717(84)90123-8

Graham, E. B., Wieder, W. R., Leff, J. W., Weintraub, S. R., Townsend, A. R., Cleveland, C. C., et al. (2014). Do we need to understand microbial communities to predict ecosystem function? A comparison of statistical models of nitrogen cycling processes. *Soil Biology and Biochemistry*, *68*, 279–282. https://doi.org/10.1016/j.soilbio.2013.08.023

Graham, E. B., Knelman, J. E., Schindlbacher, A., Siciliano, S., Breulmann, M., Yannarell, A., et al. (2016). *Microbes as engines of ecosystem function: When does community structure enhance predictions of ecosystem processes? Frontiers in Microbiology*, *7*(FEB), 1–10. https://doi.org/10.3389/fmicb.2016.00214

Grimley, D. A., Arruda, N. K., & Bramstedt, M. W. (2004). *Using magnetic susceptibility to facilitate more rapid, reproducible and precise delineation of hydric soils in the midwestern USA, 58*, 183–213. https://doi.org/10.1016/j.catena.2004.03.001

Groffman, P. M., Butterbach-Bahl, K., Fulweiler, R. W., Gold, A. J., Morse, J. L., Stander, E. K., et al. (2009). Challenges to incorporating spatially and temporally explicit phenomena (hotspots and hot moments) in denitrification models. *Biogeochemistry*, *93*(1–2), 49–77. https://doi.org/10.1007/s10533-008-9277-5

Han, P., & Bartels, D. M. (1996). Temperature dependence of oxygen diffusion in H_2O and D_2O. *The Journal of Physical Chemistry*, *100*(13), 5597–5602. https://doi.org/10.1021/jp952903y

Holtan-Hartwig, L., Dörsch, P., & Bakken, L. R. (2002). Low temperature control of soil denitrifying communities: Kinetics of N_2O production and reduction. *Soil Biology and Biochemistry*, *34*(11), 1797–1806. https://doi.org/10.1016/S0038-0717(02)00169-4

Horn, R., & Smucker, A. (2005). Structure formation and its consequences for gas and water transport in unsaturated arable and forest soils. *Soil and Tillage Research*, *82*(1), 5–14. https://doi.org/10.1016/j.still.2005.01.002

Illinois climate network. (2017). *Water and atmospheric resources monitoring program*. Champaign, IL: Illinois Water Survey. https://doi.org/10.13012/J8MW2F2Q

Jarecke, K. M., Loecke, T. D., & Burgin, A. J. (2016). Coupled soil oxygen and greenhouse gas dynamics under variable hydrology. *Soil Biology and Biochemistry*, *95*, 164–172. https://doi.org/10.1016/j.soilbio.2015.12.018

Knowles, R. (1982). Denitrification. *Microbiological Reviews*, *46*(1), 43–70.

Kool, D. M., Wrage, N., Zechmeister-Boltenstern, S., Pfeffer, M., Brus, D., Oenema, O., & Van Groenigen, J.-W. (2010). Nitrifier denitrification can be a source of N_2O from soil: A revised approach to the dual-isotope labelling method. *European Journal of Soil Science*, *61*(5), 759–772. https://doi.org/10.1111/j.1365-2389.2010.01270.x

Krichels, A., DeLucia, E. H., Sanford, R., Chee-Sanford, J., & Yang, W. H. (2019). Historical soil drainage mediates the response of soil greenhouse gas emissions to intense precipitation events. *Biogeochemistry*, *142*(3), 425–442. https://doi.org/10.1007/s10533-019-00544-x

Le, P. V. V, Kumar, P., Valocchi, A. J., & Dang, H. (2015). GPU-based high-performance computing for integrated surface sub-surface flow modeling. *Environmental Modelling and Software*, *73*, 1–13. https://doi.org/10.1016/j.envsoft.2015.07.015

Li, C., Frolking, S., & Frolking, T. A. (1992). A model of nitrous oxide evolution from soil driven by rainfall events: 1. Model structure and sensitivity. *Journal of Geophysical Research Atmospheres*, *97*(D9), 9759–9776. https://doi.org/10.1029/92JD00509

Li, J. R., Anderson, T., & Walter, M. T. (2012). Landscape scale variation in nitrous oxide flux along a typical northeastern US topographic gradient in the early summer. *Water Air and Soil Pollution*, *223*(4), 1571–1580. https://doi.org/10.1007/s11270-011-0965-8

Li, X., McCarty, G. W., Lang, M., Ducey, T., Hunt, P., & Miller, J. (2018). Topographic and physicochemical controls on soil denitrification in prior converted croplands located on the Delmarva Peninsula, USA. *Geoderma*, *309*, 41–49. https://doi.org/10.1016/j.geoderma.2017.09.003

Linn, D. M., & Doran, J. W. (1984). Effect of water-filled pore space on carbon dioxide and nitrous oxide production in tilled and nontilled soils. *Soil Science Society of America Journal*, *48*(1961), 1267–1272.

Maag, M., & Vinther, F. P. (1996). Nitrous oxide emission by nitrification and denitrification in different soil types and at different soil moisture contents and temperatures. *Applied Soil Ecology*, *4*(1), 5–14. https://doi.org/10.1016/0929-1393(96)00106-0

Matson, P. A., Vitousek, P. M., Livingston, G. P., & Swanberg, N. A. (1990). Sources of variation in nitrous oxide flux from Amazonian ecosystems. *Journal of Geophysical Research*, *95*(D10), 16,789–16,798. https://doi.org/10.1029/JD095iD10p16789

Matthias, D., Yarger, D. N., & Weinbeck, R. S. (1978). A numerical evaluation of chamber methods for determining gas fluxes. *Geophysical Research Letters*, *5*(9), 765–768.

Mbuthia, L. W., Acosta-Martínez, V., DeBruyn, J., Schaeffer, S., Tyler, D., Odoi, E., et al. (2015). Long term tillage, cover crop, and fertilization effects on microbial community structure, activity: Implications for soil quality. *Soil Biology and Biochemistry*, *89*, 24–34. https://doi.org/10.1016/j.soilbio.2015.06.016

McClain, M. E., Boyer, E. W., Dent, C. L., Gergel, S. E., Grimm, N. B., Groffman, P. M., et al. (2003). Biogeochemical hot spots and hot moments at the interface of terrestrial and aquatic ecosystems. *Ecosystems*, *6*(4), 301–312. https://doi.org/10.1007/s10021-003-0161-9

Meyer, N., Meyer, H., Welp, G., & Amelung, W. (2018). Soil respiration and its temperature sensitivity (Q10): Rapid acquisition using mid-infrared spectroscopy. *Geoderma*, *323*(July 2017), 31–40. https://doi.org/10.1016/j.geoderma.2018.02.031

Milne, A. E., Haskard, K. A., Webster, C. P., Truan, I. A., Goulding, K. W. T., & Lark, R. M. (2011). Wavelet analysis of the correlations between soil properties and potential nitrous oxide emission at farm and landscape scales. *European Journal of Soil Science*, *62*(3), 467–478. https://doi.org/10.1111/j.1365-2389.2011.01361.x

Min, S. K., Zhang, X., Zwiers, F. W., & Hegerl, G. C. (2011). Human contribution to more-intense precipitation extremes. *Nature*, *470*(7334), 378–381. https://doi.org/10.1038/nature09763

Molodovskaya, M., Singurindy, O., Richards, B. K., Warland, J., Johnson, M. S., & Steenhuis, T. S. (2012). Temporal variability of nitrous oxide from fertilized croplands: Hot moment analysis. *Soil Science Society of America Journal*, *76*(5), 1728–1740. https://doi.org/10.2136/sssaj2012.0039

Nitzsche, K. N., Kaiser, M., Premke, K., Gessler, A., Ellerbrock, R. H., Hoffmann, C., et al. (2017). Organic matter distribution and retention along transects from hilltop to kettle hole within an agricultural landscape. *Biogeochemistry*, *136*(1), 47–70. https://doi.org/10.1007/s10533-017-0380-3

Palta, M. M., Ehrenfeld, J. G., Gimenez, D., Groffman, P. M., & Subroy, V. (2016). Soil texture and water retention as spatial predictors of denitrification in urban wetlands. *Soil Biology & Biochemistry*, *101*, 237–250. https://doi.org/10.1016/j.soilbio.2016.06.011

Paradis, E., & Schliep, K. (2018). ape 5.0: An environment for modern phylogenic and evolutionary analyses in R. *Bioinformatics*, (35) 526–528.

Pett-Ridge, J., Silver, W. L., & Firestone, M. K. (2006). Redox fluctuations frame microbial community impacts on N-cycling rates in a humid tropical forest soil. *Biogeochemistry*, *81*, 95–110. https://doi.org/10.1007/s10533-006-9032-8

Philippot, L., & Hallin, S. (2005). Finding the missing link between diversity and activity using denitrifying bacteria as a model functional community. *Current Opinion in Microbiology*, *8*(3), 234–239. https://doi.org/10.1016/j.mib.2005.04.003

Philippot, L., Čuhel, J., Saby, N. P. A., Chèneby, D., Chroňáková, A., Bru, D., et al. (2009). Mapping field-scale spatial patterns of size and activity of the denitrifier community. *Environmental Microbiology*, *11*(6), 1518–1526. https://doi.org/10.1111/j.1462-2920.2009.01879.x

Pinheiro, J., DebRoy, S., Sarkar, D., & R Core Team. (2017). nlme: Linear and nonlinear mixed effects models. Retrieved from https://cran.r-project.org/package=nlme

Core Team, R. (2018). *R: A language and environment for statistical computing*. Vianna, Austria: R Foundation for Statistical Computing.

Russenes, A. L., Korsaeth, A., Bakken, L. R., & Dörsch, P. (2016). Spatial variation in soil pH controls off-season N_2O emission in an agricultural soil. *Soil Biology and Biochemistry*, *99*, 36–46. https://doi.org/10.1016/j.soilbio.2016.04.019

Saha, D., Rau, B. M., Kaye, J. P., Montes, F., Adler, P. R., & Kemanian, A. R. (2017). Landscape control of nitrous oxide emissions during the transition from conservation reserve program to perennial grasses for bioenergy. *GCB Bioenergy*, *9*(4), 783–795. https://doi.org/10.1111/gcbb.12395

Schimel, D., Stillwell, M. A., & Woodmansee, R. G. (1985). Biogeochemistry of C, N, and P in a soil catena of the shortgrass steppe. *Ecology*, *66*(1), 276–282. https://doi.org/10.2307/1941328

Sebilo, M., Mayer, B., Nicolardot, B., Pinay, G., & Mariotti, A. (2013). Long-term fate of nitrate fertilizer in agricultural soils. *Proceedings of the National Academy of Sciences*, *110*(45), 18,185–18,189. https://doi.org/10.1073/pnas.1305372110

Sexstone, A. J., Parkin, T. B., & Tiedje, J. M. (1985). Temporal response of soil denitrification rates to rainfall and irrigation. *Soil Science Society of America Journal*, *49*(1), 99. https://doi.org/10.2136/sssaj1985.03615995004900010020x

Sey, B. K., Manceur, A. M., Whalen, J. K., Gregorich, E. G., & Rochette, P. (2008). Small-scale heterogeneity in carbon dioxide, nitrous oxide and methane production from aggregates of a cultivated sandy-loam soil. *Soil Biology and Biochemistry*, *40*, 2468–2473. https://doi.org/10.1016/j.soilbio.2008.05.012

Six, J., Bossuyt, H., Degryze, S., & Denef, K. (2004). A history of research on the link between (micro)aggregates, soil biota, and soil organic matter dynamics. *Soil and Tillage Research*, *79*, 7–31. https://doi.org/10.1016/j.still.2004.03.008

Soil Survey Staff (2006). *Soil Survey Staff*, Natural Resources Conservation Service, United States Department of Agriculture. Land resource regions and major land resource areas of the United States, the Caribbean, and the Pacific Basin. Agricultural Handbook 296 digital maps and attributes. Accessed 4th Feb 2017

Sophocleous, M. (2002). Interactions between groundwater and surface water: The state of the science. *Hydrogeology Journal*, *10*(1), 52–67. https://doi.org/10.1007/s10040-001-0170-8

Suriyavirun, N., Krichels, A. H., Kent, A. D., & Yang, W. H. (2019). Microtopographic differences in soil properties and microbial community composition at the field scale. *Soil Biology and Biochemistry*, *131*, 71–80. https://doi.org/10.1016/j.soilbio.2018.12.024

Takai, Y., & Kamura, T. (1966). The mechanism of reduction in waterlogged paddy soil. *Folia Microbiologica*, *11*(4), 304–313. https://doi.org/10.1007/BF02878902

Turner, P. A., Griffis, T. J., Mulla, D. J., Baker, J. M., & Venterea, R. T. (2016). A geostatistical approach to identify and mitigate agricultural nitrous oxide emission hotspots. *Science of The Total Environment*, *572*, 442–449. https://doi.org/10.1016/j.scitotenv.2016.08.094

USGCRP (2009). Global climate change impacts in the United States. In T. R. Karl, J. M. Melillo, & T.C. Peterson (Eds.). United States Global Change Research Program. New York, NY: Cambrige University Press.

Velthof, G. L., Jarvis, S. C., Stein, A., Allen, A. G., & Oenema, O. (1996). Spatial variability of nitrous oxide fluxes in mown and grazed grasslands on a poorly drained clay soil. *Soil Biology and Biochemistry*, *28*(9), 1215–1225. https://doi.org/10.1016/0038-0717(96)00129-0

Yanai, J., Sawamoto, T., Oe, T., Kusa, K., Yamakawa, K., Sakamoto, K., et al. (2003). Spatial variability of nitrous oxide emissions and their soil-related determining factors in an agricultural field. *Journal of Environmental Quality*, *32*(6), 1965–1977. https://doi.org/10.2134/jeq2003.1965

Zogg, G. P., Zak, D. R., Ringelberg, D. B., White, D. C., MacDonald, N. W., & Pregitzer, K. S. (1997). Compositional and functional shifts in microbial communities due to soil warming. *Soil Science Society of America Journal*, *61*(2), 475. https://doi.org/10.2136/sssaj1997.03615995006100020015x